Modeling Transition in Separated and Attached Boundary Layers

Stephen K. Roberts
e-mail: skrobert@connect.carleton.ca

Metin I. Yaras
e-mail: metin_yaras@carleton.ca

Department of Mechanical and Aerospace Engineering,
Carleton University,
3135 Mackenzie Building,
1125 Colonel By Drive,
Ottawa, ON K1S 5B6, Canada

This paper presents a mathematical model for predicting the rate of turbulent spot production. In this model, attached- and separated-flow transition are treated in a unified manner, and the boundary layer shape factor is identified as the parameter with which the spot production rate correlates. The model is supplemented by several correlations to allow for its practical use in the prediction of the length of the transition zone. Second, the paper presents a model for the prediction of the location of transition inception in separation bubbles. The model improves on the accuracy of existing alternatives, and is the first to account for the effects of surface roughness. [DOI: 10.1115/1.1860570]

Keywords: Boundary Layer Transition, Transition Modeling

Introduction

Since the concept of the turbulent spot was initially proposed by Emmons [1], extensive experimental research efforts have been dedicated to uncovering the mechanisms leading to transition inception (e.g., [2–6]) and the process of growth and merging of turbulent spots into a fully turbulent boundary layer (e.g., [7–9]). Studies such as these have increased our understanding of the transition process and have identified the flow parameters that significantly affect this process, namely, freestream turbulence intensity [10,11], turbulence length scale [12,13], streamwise pressure gradients [14–16], streamline curvature [17,18], periodic impingement of wakes [19–21], and surface roughness [22,23].

The ultimate mathematical model for the transition process already exists in the form of the unsteady Navier-Stokes equations. Until relatively recently, however, lack of computing power has prevented the numerical solution of these equations with sufficient resolution to predict the details of turbulence production, convection, diffusion and dissipation in transitioning or turbulent flows. Such direct numerical simulations (DNS) are now being used as numerical wind tunnels to shed light onto fundamental features of transition and turbulence [24–27], which are extremely difficult to observe through physical experiments. However, the available computing power has imposed limits on the range of flow Reynolds numbers that can be considered in such simulations [27,28], which will remain so for the foreseeable future.

There has been considerable research focusing on predicting transition through the use of low-Reynolds-number turbulence models (e.g., [29–31]). In the authors' opinion, however, there are no fundamental grounds for these turbulence models to capture the proper physics of the transition process, for they have been tailored to predict the near-wall region of fully turbulent boundary layers. Flow phenomena key to the transition process, such as amplification of instabilities leading to the inception of turbulent spots and the distinct spreading patterns of these spots, are concealed by the Reynolds-averaging process. Nonetheless, there have been numerous attempts to make these models mimic transition phenomena by drawing analogies between the cross-stream variation of turbulence near a solid surface and the streamwise variation of turbulence during transition. Such methods employ a subgroup of models based on the turbulence Reynolds number rather than on wall proximity. Proper execution of this approach requires the presence of freestream disturbances, which limits the transition process to that of the bypass type, triggered by diffusion of freestream turbulence into the shear layer. Savill [32] showed that low-Re turbulence models fail to predict both the transition onset location and the length of the transition zone accurately. The latter trend was noted by Schmidt and Patankar [31] as well, who also showed that these models are sensitive to the streamwise start location of calculations and to the initial profiles of turbulence quantities. The poor performance of low-Reynolds-number turbulence models in attached flow is likely to prevail in separated-flow transition as well.

There have been attempts to improve the transition prediction performance of low-Reynolds-number turbulence models through the use of intermittency functions (e.g., [33]). Such methods are more general than the basic low-Reynolds-number turbulence modeling approach, in the sense that they explicitly account for spot formation and growth rates. However, the underlying assumption of similarity between the turbulence structure in the turbulent spots and in the fully turbulent boundary layer remains, and the location of transition inception needs to be estimated through other means, typically empirical correlations. Hobson and Weber [34] attempted to use the turbulence model of Spalart and Allmaras [35] together with the intermittency function of Solomon et al. [36] for separation-bubble transition and found that the internal structure of the bubble was not predicted well. More recently, transport equations have been developed for predicting the streamwise variation of intermittency rather than relying on empirical relations (e.g., [37,38]). The model of Suzen and Huang [38] also accounts for the cross-stream variation of flow intermittency. The authors reported reasonable accuracy for the prediction of the transition length, with the transition inception location determined through an empirical correlation. However, in the context of the previous discussion on the use of low-Re turbulence models to predict the turbulence generation within turbulent spots, the present authors remain doubtful of the feasibility of achieving consistent prediction accuracy with such models.

Large eddy simulation (LES) has relatively recently emerged as a compromise between the excessive computing requirements of DNS and the lack of general applicability of Reynolds-average Navier-Stokes (RANS) formulations to turbulent and transitional flows. In this method, the larger turbulent structures are computed explicitly, while the smaller scale turbulence is modeled, which is commonly referred to as sub-grid-scale modeling [39]. This approach has been shown to have the potential to provide substantially more consistent prediction of turbulent flows than has been accomplished by modeling the complete range of turbulence scales [40]. Because a large range of turbulence scales naturally develop during such simulations, prediction of transition inception

Contributed by the International Gas Turbine Institute (IGTI) of THE AMERICAN SOCIETY OF MECHANICAL ENGINEERS for publication in the ASME JOURNAL OF TURBOMACHINERY. Paper presented at the International Gas Turbine and Aeroengine Congress and Exhibition, Vienna, Austria, June 13–17, 2004, Paper No. 2004-GT-53664. Manuscript received by IGTI, October 1, 2003; final revision, March 1, 2004. IGTI Review Chair: A. J. Strazisar.

and turbulent spot propagation is theoretically within the capability of this method. This has been confirmed through case studies in the published literature (e.g., [40,41]). However, the LES computing requirements for high-Re flows are within the range that still makes LES unattractive for regular use in industry. Additionally, the feasibility of sub-grid-scale turbulence models that are equally effective away as well as in close proximity of solid boundaries remains the focus of extensive research. Hence, it will be some time before this technique matches the reliability and efficiency of the well proven semi-empirical modeling approach for the prediction of the transition process.

Based on these observations, for the foreseeable future, semi-empirical mathematical tools appear to be the most accurate and time efficient means for modeling turbulent spot inception and propagation. The present study begins with a review of existing models for predicting transition inception and transition length, and proposes models that account for the effects of a broader range of flow and geometric parameters, calibrated against an extensive set of experimental data.

Review of Semi-Empirical Transition Models

Transition from laminar to turbulent flow in boundary layers is known to take place through the inception and spreading of turbulent spots, which in planform view resemble an arrowhead, with the tip pointing in the downstream direction (e.g., [1,42]). Once formed, these spots are convected downstream while they spread in the streamwise, spanwise, and cross-stream directions, until merging with each other to form a fully turbulent boundary layer. The length of the transition zone is therefore dictated by the inception, convection, and spreading rates of the turbulent spots. For modeling purposes, the state of the boundary layer in the transition zone is conventionally described by the intermittency, γ, which is the fraction of time that a given location in the boundary layer resides within turbulent spots. Emmons [1] showed this to be a continuous Poisson process. Ignoring variations in the intermittency in the cross-stream and spanwise directions, this may be mathematically expressed as

$$\gamma(x) = 1 - e^{-\int n(x)dx \int g_x(x)dx \int g_z(x)dx} \tag{1}$$

where n represents the inception rate of turbulent spots at a given location, and g_x and g_z respectively represent the streamwise and spanwise spreading rates of these spots.

Inception of Turbulent Spots. The uniformly distributed spot production assumed in Emmons' [1] theory is not supported by the concentrated inception of spots observed in the experiments of Schubauer and Klebanoff [43]. Recently, Johnson and Fashifar [8] observed the presence of a finite streamwise band within which spot inception takes place. Nonetheless, this band is sufficiently narrow to justify Narasimha's [9] hypothesis of concentrated breakdown, whereby spot inception occurs at random times and spanwise locations at one streamwise location. Another underlying assumption in Emmons' theory is that the inception of a turbulent spot is not affected by the proximity of other spots. However, it has been demonstrated experimentally [8] that turbulent spots are less likely to be produced in close proximity of each other. This may be, in part, due to the existence of a calmed region following the passage of a turbulent spot [8,42]. Despite evidence of deviations from the assumptions of concentrated breakdown and spot formation that is uninfluenced by other spots, the level of success with transition models based on Narasimha's hypothesis [9,36] suggests these deviations to be small.

The inception of turbulent spots in an attached boundary layer is typically preceded by the growth of instability (Tollmien-Schlichting) waves, which is for the most part a linear process, becoming nonlinear shortly before breakdown into turbulent spots (e.g., [5,24]). This transition mode, known as natural transition, is encountered in relatively low disturbance environments and has recently been observed to potentially be the dominant mechanism of transition also in instances where the boundary layer separates prior to transition onset [24]. In cases of separated flow, the highly inflectional mean velocity profile downstream of the point of separation tends to substantially reduce the streamwise length of instability growth leading to transition inception (e.g., [44–46]). In an environment with large disturbances, such as elevated freestream turbulence and substantial surface roughness, the relatively long process of linear growth of instability waves is bypassed, leading to the formation of turbulent spots shortly after exposure of the laminar boundary layer to such disturbances (e.g., [10,47]).

Regardless of whether transition is of the natural or bypass mode, experimental studies have shown that the rate of turbulent spot inception is affected by the local freestream turbulence and streamwise pressure gradient [14,48], and surface roughness, as indicated indirectly by the measurements of Pinson and Wang [23]. The random occurrence of turbulent spots prevents direct measurement of their inception rates. Thus, conclusions regarding the trends in spot inception rates have been deduced from the transition length and spot propagation characteristics in the transition zone. The level of success in experimentally quantifying the inception rate of turbulent spots is therefore closely coupled to the extent of our understanding of their convection and spreading characteristics.

Convection and Spreading of Turbulent Spots. Since the work of Emmons [1], numerous studies have documented the development of turbulent spots as they are convected downstream. These studies measured the structure and spreading of spots in the horizontal plane (e.g., [7,49]) or in the vertical plane of symmetry [7]. More recently, measurements have been undertaken to fully document the three-dimensional spot structure (e.g., [42]). Such three-dimensional measurements have identified distinct regions of turbulence generation at the leading edge and along the lateral extremes of the spots. Through these studies, the local pressure gradient has been confirmed as the parameter dominating the spreading rate of turbulent spots.

Transition Models.

Location of Transition Inception. In attached boundary layers, the widely accepted parameter for correlating the location of transition inception is the Reynolds number based on momentum thickness, Re_θ. Among the numerous transition inception formulations, those of Mayle [50] (Eq. (2)) and Abu-Ghannam and Shaw [3] (Eqs. (3)) are the ones cited most frequently in turbomachinery blade studies.

$$\mathrm{Re}_{\theta ts} = 400\, Tu^{-0.625} \tag{2}$$

$$\mathrm{Re}_{\theta ts} = 163 + \exp\left(F(\lambda_\theta) - \frac{F(\lambda_\theta)}{6.91}\overline{Tu}\right) \tag{3a}$$

where $\mathrm{Re}_{\theta ts}$ is the Reynolds number based on momentum thickness at the transition inception location, $\overline{Tu}$ is the average freestream turbulence level between the leading edge and transition inception location, and $F(\lambda_\theta)$ in Eq. (3*a*) is a function of Thwaites' pressure gradient parameter $(\lambda_\theta = (\theta^2/\nu)dU_e/dx)$, defined as

$$F(\lambda_\theta) = 6.91 + 12.75\lambda_\theta + 63.64\lambda_\theta^2 \quad \{\lambda_\theta \leqslant 0\} \tag{3b}$$

$$F(\lambda_\theta) = 6.91 + 2.48\lambda_\theta - 12.27\lambda_\theta^2 \quad \{\lambda_\theta \geqslant 0\} \tag{3c}$$

Although the model of Abu-Ghannam and Shaw [3] has the advantage of accounting for the effects of both freestream turbulence and streamwise pressure distribution, for flows with high turbulence intensity it has been artificially forced to correspond to the stability limit for natural transition of $\mathrm{Re}_{\theta ts} = 163$. Mayle's [50] correlation is not constrained by this stability limit, but it does not account for the effects of pressure gradient. For freestream turbulence intensities typical of turbomachinery blade rows, it is known

that transition inception in an attached boundary layer is not strongly affected by the streamwise pressure distribution [13,50]. Thus, Eq. (2) is suitable for such applications. The experimental results from an earlier phase of the present research [13], covering a range of pressure gradients and freestream turbulence levels, were predicted reasonably well by both of these models.

For transition in short separation bubbles, the location of transition inception has been found to correlate well with the state of the boundary layer at the point of separation.

Mayle [50]

$$\mathrm{Re}_{ts} - \mathrm{Re}_s = 300\,\mathrm{Re}_{\theta s}^{0.7} \tag{4}$$

where Re_s and Re_{ts} are the Reynolds numbers based on the streamwise locations of separation (x_s) and transition inception (x_{ts}), respectively.

Roberts [51]

$$\mathrm{Re}_{s-ts} = 2.5 \times 10^4 \log_{10}\{\coth[TF(\%)/10]\} \tag{5}$$

In this equation, TF is Taylor's [52] turbulence factor [$TF = Tu_{\mathrm{ref}}(L/\lambda_s)^{0.2}$], where λ_s is the integral length scale of freestream turbulence, and L is the length of the surface along which the boundary layer develops.

Hatman and Wang [44]

$$\mathrm{Re}_{ts} = 1.0816\,\mathrm{Re}_s + 26{,}805 \tag{6}$$

Yaras [53]

$$\mathrm{Re}_{ts} = 1.04\,\mathrm{Re}_s + 6.3 \times 10^4\{1 - \tanh^3[TF'(\%)]\} \tag{7}$$

where $TF' = \max[TF, (\%)1\%]$.

Among these models, the latter two have been found to be more accurate when compared to the experimental transition data that have been measured at Carleton University over the past several years [45,53,54]. While the models of Hatman and Wang [44] and Yaras [53] agree well with each other at low freestream turbulence levels, only the latter model is applicable to elevated free-stream turbulence conditions.

Length of Transition. Early efforts to model the transition region for attached boundary layers (e.g., [1,9]), did so without the benefit of more refined measurements of streamwise propagation rates and spreading angles that have become available more recently [7,42,49]. Nonetheless, the concentrated breakdown hypothesis described earlier, along with the further assumption of constant spreading rates in the streamwise and lateral directions, led to the well-known intermittency model of Narasimha [9]:

$$\gamma(x) = 1 - e^{-(n\sigma/U_e)(x - x_{ts})^2} \quad \{x \geqslant x_{ts}\} \tag{8}$$

where n is the spot inception rate and σ is a spot propagation parameter given by

$$\sigma = U_e(U_{TE}^{-1} - U_{LE}^{-1})\tan(\alpha) \tag{9}$$

In Eq. (9), α is the lateral spot spreading half-angle, and U_{LE} and U_{TE} are the spot leading- and trailing-edge convection velocities, respectively.

*Spot Inception Rate***.** Narasimha [9] proposed a nondimensional inception rate parameter formulated as

$$N = \frac{n\sigma\theta_{ts}^3}{\nu} \tag{10}$$

Based on experimental data primarily for low values of λ_θ [2,3,43,55], Narasimha proposed a value of $N = 0.7 \times 10^{-3}$, for freestream turbulence levels above 0.1%.

More recently, Fraser et al. [14] established a dependence of N on both streamwise pressure gradient and turbulence level through experimental data compiled from various sources and proposed the following model:

$$N = \frac{47.23 \times 10^{-3}}{(10 - e^{1.7 - \mathrm{Tu}/2})^2} \times e^F \tag{11a}$$

$$F = -10\sqrt{\lambda_{\theta ts}} + 300{\lambda_{\theta ts}}^4 \quad \{\lambda_{\theta ts} \geqslant 0\} \tag{11b}$$

$$F = \lambda_{\theta ts}(1 - 55{\lambda_{\theta ts}}^2) \times (2.6\mathrm{Tu} + 3.6\sqrt{\mathrm{Tu}} - 86) \quad \{\lambda_{\theta ts} \leqslant 0\} \tag{11c}$$

Based on additional experimental data, Gostelow et al. [48] suggested the following alternative expressions for N:

$$N = 8.6 \times 10^{-4} e^{2.134\lambda_{\theta ts}\ln \mathrm{Tu}_{ts} - 59.23\lambda_{\theta ts} - 0.564 \ln \mathrm{Tu}_{ts}} \{\lambda_{\theta ts} \leqslant 0\} \tag{12a}$$

$$N = 8.6 \times 10^{-4} e^{-0.564 \ln \mathrm{Tu}_{ts} - 10\sqrt{\lambda_{\theta ts}}} \quad \{\lambda_{\theta ts} \geqslant 0\} \tag{12b}$$

In experiments by the present authors [13], Eq. (12*b*) was found to provide accurate predictions of the spot production rates, while Eq. (12*a*) was found to overestimate these measurements. Replacement of the factor 8.6 in Eq. (12*a*) with 3.0 provided a better agreement between measurements and predictions [13], although this created a slight discontinuity at $\lambda_{\theta ts} = 0$.

*Spot Propagation Rate***.** The intermittency model of Narasimha (Eq. (8)) has been found to agree well with measurements in flows with both favorable and mild adverse pressure gradients (e.g., [9,48,56]), provided that the pressure gradient does not vary significantly within the transition region. If the pressure gradient varies significantly within the transition region, which is often the case with turbomachinery blades, then the intermittency distribution may deviate from the distribution given by Eq. (8). Chen and Thyson [57] postulated that this discrepancy is due to changes in the convection velocity of the turbulent spots, caused by the streamwise pressure gradient, and suggested that their rate of convection should scale on the local freestream velocity. However, Walker et al. [58] noted that this adjustment is insufficient to establish good agreement with experimental results.

The failure of the model of Chen and Thyson [57] is attributed to the fact that the streamwise and spanwise spreading rates of turbulent spots vary significantly with λ_θ, as was documented by Gostelow et al. [7]. Based on these findings, Solomon et al. [36] proposed the following expression:

$$\gamma = 1 - e^{-n\int_{x_{ts}}^{x}[\sigma/\tan(\alpha)U]dx\int_{x_{ts}}^{x}\tan(\alpha)dx} \tag{13}$$

In this equation, $\sigma/[\tan(\alpha)U]$ and $\tan(\alpha)$ represent the streamwise and spanwise spreading of turbulent spots, respectively. Based on the experimental data compiled by Gostelow et al. [7] for λ_θ values between −0.06 and 0.06, the following expressions for the spot-spreading characteristics were proposed:

$$a = 4 + 22.14/(0.79 + 2.72e^{47.63\lambda_\theta}) \tag{14}$$

$$\sigma = 0.03 + 0.37/(0.48 + 3.0e^{52.9\lambda_\theta}) \tag{15}$$

More recently, Eq. (15) was updated by D'Ovidio et al. [59] to extend the range of λ_θ to −0.12:

$$\sigma = 0.024 + 0.604/(1 + 5e^{66\lambda_\theta}) \tag{16}$$

Experiments by the present authors [13], conducted over a range of pressure distributions, freestream turbulence, and flow Reynolds numbers, provided indirect evidence that these spot propagation parameters are adequately described by the pressure gradient parameter, without any need for further adjustment due to freestream turbulence and Reynolds number.

Johnson and Ercan [12] proposed an alternative approach for modeling the intermittency distribution in the transition zone, with a focus on conditions with elevated levels of freestream turbulence ($Tu > 2\%$). The model relaxes the assumption of concentrated spot production, and bases the spot production rate on the near-wall and freestream turbulence length scales in addition to

Table 1 Summary of experimental configurations

Study	Test-section config.	$Re_L(\times 10^5)$	$Tu_{ref}(\%)$	Smooth surface	Rough surface	C_p dist.	Hotwire type
RY	Flat plate	3.5–9.3	0.5–9.0	×	×	Adv., blade	Single
VSP	Flat plate	3.5	8.7	×		Fav.	X-wire
V	Cascade	1.0–3.0	8.7	×		Blade	X-wire
VH	Flat plate	0.5–3.0	7.0	×		Fav.	Single
DV	Flat plate	13.9–18.3	1.4–3.9*	×		Fav., adv.	Single

*Estimated from turbulence grid and test section geometry

the local freestream turbulence intensity and pressure gradient. The model also includes new expressions for the spot propagation parameter σ and spreading angle α, although these differ from the predictions based on Eqs. (14) and (16) mostly for high adverse pressure gradients ($\lambda_\theta < -0.10$). The model was validated through comparisons with experimental data published by Gostelow and his co-workers. Compared to the model of Solomon et al. [36] (Eq. (13)), prediction of the intermittency distribution was improved in the early and late stages of transition.

Finally, there appears to be a substantial lack of effort on modeling the transition length in separation bubbles. As the location of reattachment is generally well correlated with the completion of transition, and the reattachment location is the more relevant information for the prediction of the downstream boundary layer development, the tendency has been to develop correlations for the reattachment location instead. Two recently proposed models are as follows:

Hatman and Wang [44]

$$\mathrm{Re}_r = 1.0608\,\mathrm{Re}_s + 34{,}890 \tag{17}$$

Yaras [53]

$$\mathrm{Re}_r = 1.04\,\mathrm{Re}_s + 8.05 \times 10^4[1 - \tanh^3(TF'(\%))] - 2.0 \times 10^4 \tag{18}$$

where $TF' = \max[TF(\%), 1\%]$.

The uncertainty of the experimental data on which these correlations are based is expected to be somewhat higher than for the locations of separation and transition inception. This is because of the unsteady nature of the reattachment location and the greater subjectivity involved in interpreting the location of reattachment through the shape of the time-averaged velocity profile, a peak in the turbulence intensity, or a combination of the two. It would therefore be useful to establish correlations for the intermittency distributions in the separated shear layer from which the end of the transition process can be deduced with higher precision. In recent studies by the current authors [54], Volino [60], and Gostelow and Thomas [61], intermittency distributions in separation bubbles have been measured with sufficient streamwise resolution to provide the experimental basis for the development of such mathematical models.

Description of Experiments

The experimental data compiled herein have been extracted mostly from the authors' own studies [13,54] (identified by RY, as in Table 1). In order to confirm the absence of any trends in these results that may be unique to the wind tunnel and instrumentation used by the authors, results from several other research facilities have been included in the data set. The additional data are those published by Volino and co-workers (VH, VSP) [11,62], Volino (V) [60], and Devasia (DV) [56]. The data set encompasses a range of flow Reynolds numbers, streamwise pressure gradients, freestream turbulence levels, and surface roughness conditions that are typical of gas turbine applications, and includes cases with attached flow [11,13,56,62] and separation-bubble transition [54,60].

With the exception of the most recent experiments of Volino (V) [60], the noted wind-tunnel transition studies were performed using a flat test surface, with a well-defined location for the beginning of the boundary layer development. In each case, streamwise pressure distributions were imposed the test surface through the use of a contoured test-section ceiling. The ceiling was configured to yield streamwise pressure gradients that are favorable [11,56,62], adverse [13,56], or resemble those typically encountered on the suction surface of turbine blades [13,54,60]. The test surfaces were wide enough to ensure two-dimensional flow development at the spanwise locations of the boundary layer measurements. Variations in freestream turbulence were realized by the use of turbulence-generating grids, placed sufficiently upstream of the test surface to yield isotropic and homogeneous turbulence. Surface roughness variations, which were limited to the studies of the present authors, were achieved through the use of commercially available materials that provided random roughness patterns.

The experiments of Volino (V) [60] were performed in a single-passage rectilinear cascade test section. The blade geometry was chosen such that the Pak-B pressure distribution was reproduced in an incompressible flow. Through comparison of the transition trends prevailing on this blade to those observed on flat surfaces in the remainder of the studies considered here, the effects of convex surface curvature on boundary layer transition may be inferred. Only three of the ten test cases published by Volino [60] are included in the current study, namely those with high freestream turbulence and Reynolds numbers based on the suction surface length of 100,000–300,000. In the remaining seven test cases, the transition process occurred too rapidly to yield intermittency distributions with sufficient streamwise resolution for the purposes of the present study.

The noted experimental data sets are summarized in Table 1. The relevant flow parameters from the authors' previous studies [13,54,63,64] are presented in Tables 2 and 3. Three different pressure distributions were investigated in these studies; the pressure distributions identified as C_{p1} and C_{p2} are similar to those prevailing on the suction side of low-pressure turbine blades. The initial acceleration for these two pressure distributions is approximately the same, but the subsequent adverse pressure gradient is stronger in the case of the C_{p1} distribution. The designation C_{p3} corresponds to a nearly constant adverse pressure gradient that begins at the leading edge of the test surface and is milder than that encountered in the downstream portions of the C_{p1} and C_{p2} pressure distributions. Streamwise distributions of the acceleration parameter $(\eta = (\nu/U_e^2)dU_e/dx)$ corresponding to these pressure distributions are given in Fig. 1.

Proposed Transition Model

Location of Transition Inception. As shown in Fig. 2, the experimental results from earlier phases of the present research [13], covering a range of favorable and adverse pressure gradients, and freestream turbulence levels between 1.7% and 3.3% are predicted reasonably well by the model of Abu-Ghannam and Shaw [3], given by Eq. (3) in the previous section and shown by

Table 2 Flow parameters at transition inception: Attached-flow test cases [13,54,63,64]

C_p Dist.	$Re_L(\times 10^3)$	Re_{kts}	$k_{rms}/\theta_{ts}(\times 10^{-3})$	Tu_{ref} (%)	TF (%)	$\eta_{ts}(\times 10^{-7})$	$\lambda_{\theta ts}(\times 10^{-2})$	$Re_{\theta ts}$	H_{ts}	$\log_{10}(N)$
1	350	0.3	2.0	6.4	14.0	33.2	9.5	167	1.7	−4.1
1	350	109	347	4.5	11.2	−12.5	−12.2	312	2.2	−0.1
1	470	0.4	2.3	4.4	11.2	31.2	11.4	191	1.8	−3.6
1	470	0.3	1.6	6.8	15.7	33.2	12.8	199	1.7	−3.8
1	470	37	131	2.4	5.3	6.6	5.2	278	1.9	−3.5
1	470	22	89	4.1	10.3	−5.2	−3.1	245	2.0	−2.4
1	470	40	141	4.1	10.2	−2.1	−1.7	286	2.0	−2.4
1	470	145	411	2.5	5.8	−16.3	−20.5	354	2.5	−0.2
1	470	151	568	4.5	11.2	−11.3	−8.1	266	2.1	−1.2
2	350	0.3	1.9	8.9	20.8	32.3	10.1	177	1.7	−3.8
2	470	0.4	2.2	6.8	15.1	37.7	11.1	171	1.8	−3.9
2	470	0.3	1.8	9.0	21.0	39.6	13.7	185	1.6	−3.8
3	350	0.2	0.9	2.3	6.7	−6.5	−3.4	227	2.6	−2.4
3	350	0.2	0.9	3.7	8.0	−8.4	−4.6	226	2.6	−2.7
3	350	0.2	1.1	4.3	11.3	−10.9	−3.4	176	2.3	−3.0
3	350	0.2	1.8	6.2	13.2	−9.4	−1.4	122	2.2	−3.8
3	470	0.2	1.2	2.2	6.0	−7.5	−4.3	239	2.6	−2.8
3	470	0.6	2.9	3.9	9.4	−8.5	−5.6	258	2.4	−3.0
3	470	0.3	1.9	4.4	11.4	−6.1	−1.3	141	2.2	−3.6
3	470	0.3	2.6	6.1	13.1	−7.7	−0.8	98	2.1	−3.8
3	650	0.3	0.9	0.7	0.9	−5.0	−6.6	364	2.9	−1.7
3	650	0.4	1.7	2.5	6.3	−7.0	−3.3	216	2.4	−2.9
3	650	0.4	2.0	3.8	9.0	−6.2	−3.2	226	2.2	−2.8
3	650	0.4	2.7	4.6	11.9	−3.4	−0.7	139	2.1	−3.6
3	930	0.5	1.5	0.5	0.6	−4.2	−5.1	351	2.8	−1.5
3	930	0.3	1.6	3.8	9.6	−1.9	−0.6	175	2.1	−3.4
3	930	0.5	3.2	6.5	14.0	−4.3	−1.3	168	1.9	−3.7

the solid lines in Fig. 2. This agreement is achieved without having to adjust the value of $Re_{\theta ts}$ predicted by the model to account for a bias created by the measurement technique of Abu-Ghannam and Shaw [3], as suggested by Fraser et al. [14] and Dey and Narasimha [65]. It must be recognized, however, that the scatter in the data observed in Fig. 2, which is comparable to the scatter of the original data set of Abu-Ghannam and Shaw [3], translates into an uncertainty in the predicted Re_θ at transition onset of 15–20%. This level of precision may be inadequate in certain instances. For example, for the separation-bubble transition measurements of the present authors [54], where the streamwise pressure distribution is typical of the suction side of a turbine blade, the model of Abu-Ghannam and Shaw [3] predicts attached flow transition instead. Such a difference could be critical in the estimation of profile losses and heat transfer patterns on a turbine blade. The transition process in separation bubbles was shown by Yaras [45] to be sensitive to the pressure gradient history of the boundary layer prior to separation. Since this is most probably the result of the effect of such history on the streamwise development of instabilities in the boundary layer, similar effects are just as likely in instances of attached-flow transition. Such effects cannot be accounted for with the parameters currently appearing in the model of Abu-Ghannam and Shaw [3]. Thus, although this model is in fair agreement with the data of the present authors, and is

Table 3 Flow parameters at separation and transition inception: Separation-bubble test cases [13,54,63,64]

$Re_L(\times 10^3)$	$k_{rms}/\theta_s(\times 10^{-3})$	Re_{ks}	Tu_{ref} (%)	TF (%)	$\eta_s(\times 10^{-7})$	$\lambda_{\theta s}(\times 10^{-2})$	$Re_{\theta s}$	$Re_s(\times 10^3)$	$Re_{ts}(\times 10^3)$	$Re_{s-ts}(\times 10^3)$	$Re_r(\times 10^3)$	H_s	H_{ts}	$\log_{10}(N)$
350	1.3	0.3	0.6	1.7	−4.7	−3.3	263	244	285	34	271	3.1	8.1	0.5
350	1.4	0.4	0.6	1.2	−9.6	−6.4	258	261	302	36	293	3.2	8.7	0.3
350	1.3	0.3	2.2	5.9	−15.8	−10.1	252	242	271	32	280	3.0	6.4	0.6
350	1.3	0.4	4.2	8.9	−10.3	−8.4	285	270	280	23	274	3.0	4.3	0.1
350	62	16	0.7	1.4	−22.5	−13.8	257	255	289	30	295	3.0	4.2	0.9
350	66	17	2.2	5.6	−3.8	−3.0	258	273	286	31	302	3.0	5.7	0.3
350	56	16	4.4	10.8	−8.1	−6.5	288	268	273	7	274	3.0	3.3	−0.6
350	110	28	0.7	1.3	−15.4	−10.2	257	264	287	35	284	3.1	5.6	0.5
350	97	28	2.2	5.4	−16.8	−13.9	287	266	278	19	280	3.0	4.5	−0.2
350	94	29	4.2	10.3	−13.5	−13.4	314	286	287	4	294	2.9	3.2	−0.4
350	347	99	0.7	1.7	−16.7	−13.8	286	271	280	17	278	3.5	4.7	0.2
350	340	109	2.4	6.2	−24.4	−24.9	321	309	312	4	309	3.7	3.6	−0.2
470	1.6	0.5	0.4	0.7	−6.2	−5.8	306	339	390	45	357	3.1	6.8	0.8
470	1.6	0.5	0.4	0.6	−8.2	−7.7	305	349	392	47	390	3.0	7.3	0.7
470	1.5	0.5	2.3	5.9	−11.5	−11.1	309	339	362	38	359	3.0	5.2	0.6
470	1.5	0.5	3.4	8.4	−9.1	−9.0	312	336	356	31	342	2.9	4.4	0.3
470	78	25	0.6	0.8	−13.5	−13.4	316	410	448	38	438	3.1	5.7	0.9
470	49	22	2.3	5.4	−16.6	−32.7	444	362	372	17	367	2.8	3.2	0.3
470	98	37	0.5	0.7	−11.3	−16.2	376	352	380	35	378	3.0	5.3	0.3
470	405	137	0.6	0.9	−13.7	−15.8	338	378	381	8	383	3.5	4.2	−0.1

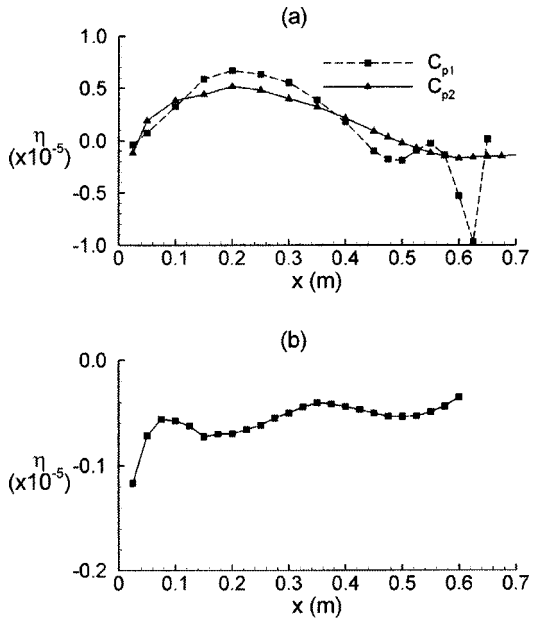

Fig. 1 Representative distributions of the acceleration parameter η for the test cases of Roberts and Yaras [13,54,63,64]: (*a*) C_{p1} and C_{p2} pressure distributions, (*b*) C_{p3} pressure distribution

herein put forward as the one favored over alternative models available in the published literature, the potential for further improvements remains.

The data points identified by the grey symbols in Fig. 2 correspond to surfaces with a range of distributed roughness with heights of approximately $0.1 < k_{\rm rms}/\theta_{ts} < 0.6$. The physics of the observed effect of surface roughness on the location of transition inception is discussed elsewhere [63,64]. Although a significant effect of roughness on $\mathrm{Re}_{\theta ts}$ is evident, the relative sparseness of the data set prevents reliable enhancement of Abu-Ghannam and Shaw's [3] model. Further measurements are needed before attempting such improvements that would make the model more relevant for the performance prediction of in-service gas turbine blades.

In instances of transition in separation bubbles, the correlation of Yaras [53] (Eq. (7)) provides reliable estimates of the location of transition inception, including cases with elevated levels of freestream turbulence. The model mimics the empirical trend of reduced sensitivity of Re_{ts} to freestream turbulence as *Tu* increases. Re_x typically does not vary significantly between the separation and transition inception locations. This is due to the

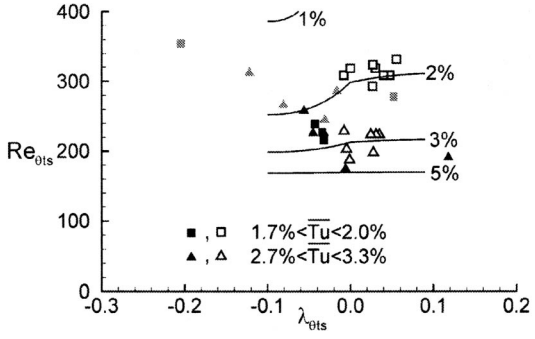

Fig. 2 Comparison of present experimental results (filled symbols) to the experimental data (hollow symbols) and correlation (lines) of Abu-Ghannam and Shaw [3]. (The present rough-surface test cases are shown in grey.)

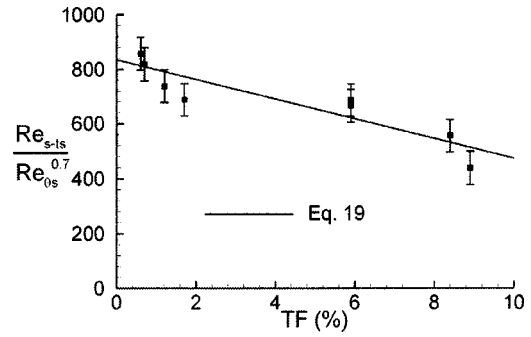

Fig. 3 Sensitivity of the transition inception location in the separation bubble to freestream turbulence (smooth surfaces)

decreasing freestream velocity partially offsetting the increase in the streamwise coordinate *x*. As a result, it is more difficult to capture the slight upstream movement of the transition inception point with increasing freestream turbulence at elevated levels of turbulence through a correlation based on Re_{ts}. This can be better accomplished if the dependent parameter Re_{ts} is replaced with the Reynolds number based on the streamwise distance between the separation and transition inception locations Re_{s-ts}. Re_{s-ts} correlates closely with the Reynolds number at the separation point $\mathrm{Re}_{\theta s}$ and decreases with increasing freestream turbulence as shown in Fig. 3. The proposed correlation is

$$\mathrm{Re}_{s-ts} = [835 - 36TF(\%)]\mathrm{Re}_{\theta s}^{0.7} \tag{19}$$

Recent experiments by the authors identified the effects of distributed surface roughness on the location of transition inception in separation bubbles [63,64]. This effect is demonstrated in terms of the parameters of the proposed model in Fig. 4. The upstream movement of the transition point with increased surface roughness height is clearly evident, and the rate of this movement appears to increase somewhat with freestream turbulence. The proposed transition-inception model (Eq. (19)) can be made to account for surface roughness effects through the following modification:

$$\mathrm{Re}_{s-ts} = \left\{835 - 36TF(\%) - [1{,}400 + 25e^{0.45TF(\%)}]\frac{k_{\rm rms}}{\theta_s}\right\}\mathrm{Re}_{\theta s}^{0.7} \tag{20}$$

Length of Transition. The proposed transition length model is based on the following expression for the streamwise intermittency distribution [36]:

$$\gamma = 1 - e^{-n\int_{x_{ts}}^{x}[\sigma/\tan(\alpha)U]dx\int_{x_{ts}}^{x}\tan(\alpha)dx} \tag{21}$$

As was noted earlier, this expression has its roots in the work of Emmons [1] and has been brought to the present level of formulation through the studies of Narasimha [9] and Solomon et al.

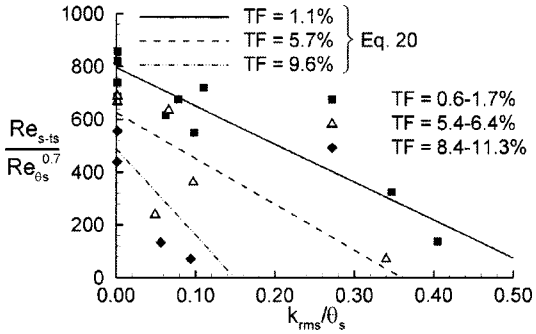

Fig. 4 Sensitivity of the transition inception location to surface roughness and freestream turbulence

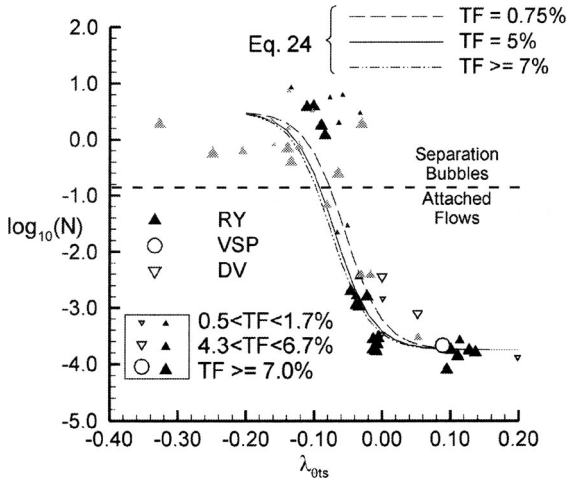

Fig. 5 Variation of the spot inception parameter with $\lambda_{\theta ts}$ and Taylor's turbulence factor. (Rough surface measurements [63,64] are shown in grey.)

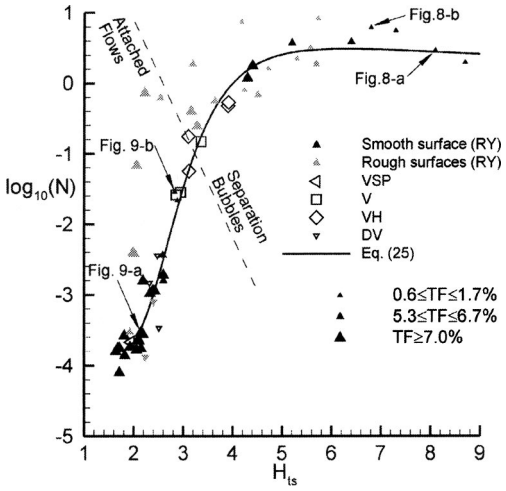

Fig. 6 Variation of the spot production parameter with the shape factor at transition inception. (Symbols filled in grey indicate measurements over a rough surface.)

[36]. Since this formulation for intermittency has been demonstrated to be consistent with the physics of the transition process based on numerous experimental studies, it has been adopted in the present modeling effort. The length of the transition zone is quantified through the streamwise distance over which Eq. (21) yields intermittency values greater than 0 and less than 1. The location of transition inception x_{ts} appearing in this expression is obtained from the models proposed in the previous section. The parameters σ and α representing the spot spreading rate are obtained from the following expressions, as proposed by Solomon et al. [36] and D'Ovidio et al. [59]:

$$a = 4 + 22.14/(0.79 + 2.72e^{47.63\lambda_\theta}) \tag{22}$$

$$\sigma = 0.024 + 0.604/(1 + 5e^{66\lambda_\theta}) \tag{23}$$

The intermittency distributions based on the experimental results of the present authors for a range of streamwise pressure gradients, freestream turbulence levels, and surface roughness conditions [13,54,63,64] have been found to be consistent with the dependence of α and σ on only λ_θ. This has been observed to be true in both attached-flow [13,63] and separated-flow [54,63,64] transition. The remaining parameter required for estimating the intermittency distribution through Eq. (21) is the spot inception rate n. As was discussed previously, starting with the work of Narasimha [9], this parameter has traditionally been extracted from the nondimensional inception rate parameter, $N = n\sigma\theta_{ts}^3/\nu$, and the most recent model, as given by Eq. (12) (with Eq. (12*a*) scaled as per the authors' recent experimental results) correlate this parameter to λ_θ and freestream turbulence at the transition inception location. Figure 5 presents measured results for the variation of N with λ_θ and freestream turbulence level. The majority of the data points, as identified with filled symbols, were measured by the present authors [13,54,63,64] and are observed to be consistent with the results of others. In the figure, the size of the symbols increases with increasing freestream turbulence level. Unlike the earlier data sets used for correlating N to λ_θ and freestream turbulence, Fig. 5 includes results from transition in separation bubbles. In the figure, the attached-flow and separated-flow transition regimes are separated approximately by a straight dashed line. Despite somewhat larger scatter, the rate of spot production is observed to remain fairly constant in separation-bubble transition for the displayed ranges of magnitudes of λ_θ and freestream turbulence. Equation (12), on the other hand, would predict a linear increase in $\log_{10}(N)$ with increasing adverse pressure gradient, rather than leveling off as suggested by the data. As a result, the following correlation is proposed, which is consistent with the experimental results throughout the $\lambda_{\theta ts}$ range of Fig. 5,

$$\log_{10}(N) = -3.75 + \frac{8.5}{2 + 35e^{35[\lambda_\theta - f(TF)]}} \tag{24a}$$

$$f(TF) = \frac{2.9 - 0.25TF(\%)}{100 + 1.4TF(\%)[1 + TF(\%)]} \tag{24b}$$

This correlation is formulated such that it provides similar results to Eq. (12) in the −0.1 to 0.08 $\lambda_{\theta ts}$ range, for turbulence intensities varying from 0.5% to 6.5%, since this earlier correlation was calibrated against an extensive data set in this range. The turbulence intensity *Tu*, appearing in the earlier expressions for *N*, is now replaced by *TF*. This was done in recognition of the fact that the effect of turbulence intensity on the transition process ought to be influenced by the length scale of the freestream turbulence eddies. In the absence of length-scale information for freestream turbulence, Eq. (24) may still be used to obtain estimates of *N* by using *Tu* in place of *TF*. The data points shown with grey symbols in Fig. 5 correspond to a range of rough-surface conditions and will be discussed shortly.

A more effective approach to estimating the spot production rate parameter *N* is evident from the results shown in Fig. 6. Excluding the rough-surface conditions identified by grey symbols, a strong dependence of *N* on the boundary-layer shape factor at the point of transition inception is observed. This is consistent with the established dependence of *N* on the freestream turbulence level and streamwise pressure gradient, for both factors are known to affect the shape factor. However, the notably lower scatter in Fig. 6 than that observed in Fig. 5 may suggest the boundary layer shape factor to be more directly relevant to the rate of turbulent spot production. The trends in Fig. 6 suggest the following correlation between N and H_{ts}:

$$\log_{10}(N) = \frac{0.55H_{ts} - 2.2}{1 - 0.63H_{ts} + 0.14H_{ts}^2} \quad \{1.6 \leq H_{ts} \leq 8.5\} \tag{25}$$

The use of this correlation to estimate N requires that H_{ts} be known. In instances of attached-flow transition, this information can be obtained most efficiently by the use of an integral method, such as the method of Thwaites [66], for the streamwise development of the laminar boundary layer up to the point of transition inception. Based on the data published by White [67], H can be correlated to λ_θ through

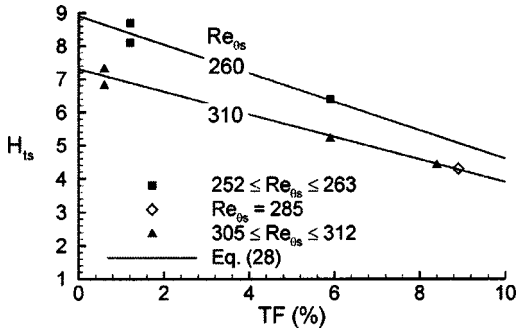

Fig. 7 Variation of H_{ts} with turbulence level and $Re_{\theta s}$ for separation-bubble transition (smooth surfaces)

$$H = \frac{2.61 + 20.3\lambda_\theta}{1 + 9.43\lambda_\theta + 8.35\lambda_\theta^2} \quad \{-0.09 \leq \lambda_\theta \leq 0.25\} \qquad (26)$$

The effect of freestream turbulence on H is not accounted for in this empirical correlation and can be estimated from the following expression, which is based on the experimental results of the present authors:

$$\frac{H}{H_T} = 1 - 0.03TF(\%) \quad \{TF(\%) \leq 11\} \qquad (27)$$

where H_T is the shape factor estimated from Eq. (26).

For estimating the shape factor at the point of transition inception in separation bubbles, the following correlation is proposed for smooth surfaces, over the ranges of $250 \leq Re_{\theta s} \leq 310$ and $TF \leq 10\%$, based on the experimental data shown in Fig. 7.

$$H_{ts} = (17.2 - 0.032\,Re_{\theta s}) - (0.9 - 0.0018\,Re_{\theta s})TF(\%) \qquad (28)$$

In summary, the proposed model for predicting the length of the transition zone, unified for attached- and separated-flow transition, consists of Eqs. (21)–(23) and (25). These are supplemented by Eqs. (3) or (20) to predict the streamwise location of transition inception, by Eq. (10) to relate n to N, and by Eqs. (26)–(28) to predict the shape factor at this point, if necessary.

For two of the separated-flow transition cases labeled in Fig. 6, the predicted intermittency distribution, hence, transition length, is compared to the measured values in Fig. 8 The spot production parameter N of the test case corresponding to Fig. 8(*b*) is off of the trend line (Eq. (25)) in Fig. 6 by about one standard deviation. Thus, the difference in the extent of agreement of the predicted and experimental intermittency distributions in Fig. 8 provides an indication of the effect of the scatter in the measured values of N on the prediction accuracy of the transition length. This effect is noted to be relatively small.

Similarly, the measured and predicted intermittency distributions for two attached-flow transition cases (labeled in Fig. 6) are compared in Fig. 9. Again, Fig. 9(*b*) corresponds to a test case that represents the extent of scatter in the measured values of N. The effect of the uncertainty in the N values on the prediction accuracy of the transition length is observed to be small. For reference, the predictions based on N values estimated through Eq. (12), with Eq. (12*a*) modified as per the authors' recent observations [13], are also included in these figures. Since both Eqs. (12) and (25) are calibrated against the same attached-flow transition data set, the accuracy of the prediction is similar with the two models.

Effect of Surface Roughness on Transition Length. For attached-flow transition, presence of roughness is noted to increase N for a given $\lambda_{\theta ts}$ (Fig. 5) or H_{ts} (Fig. 6). This trend is particularly evident in Fig. 6, where H_{ts} assumes a nearly constant value of 2 for the attached-flow transition cases over rough surfaces. The rough-surface data points shown in the figure for attached-flow transition correspond to a range of roughness

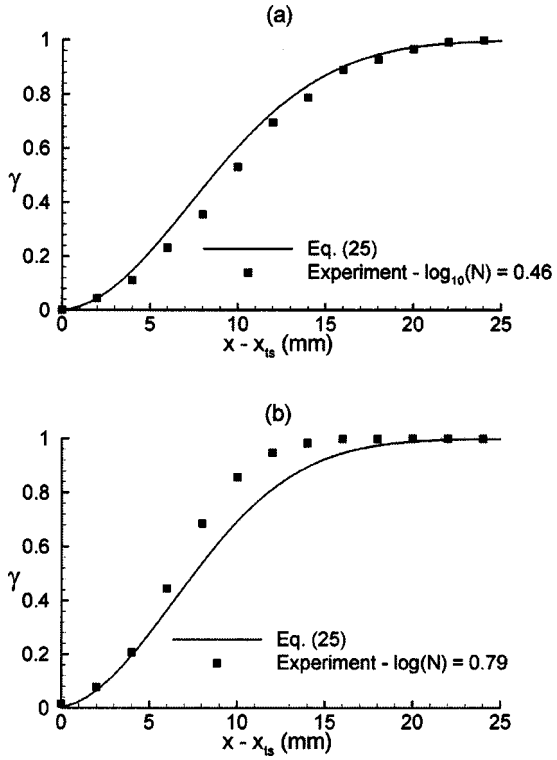

Fig. 8 Intermittency distributions for two separated-flow transition cases (as labeled in Fig. 6)

heights of about $0.1 < k_{rms}/\theta_{ts} < 0.6$, with a trend toward increasing spot production rate with increasing height of roughness elements. It therefore appears that although freestream turbulence affects the spot production rate primarily through its influence on

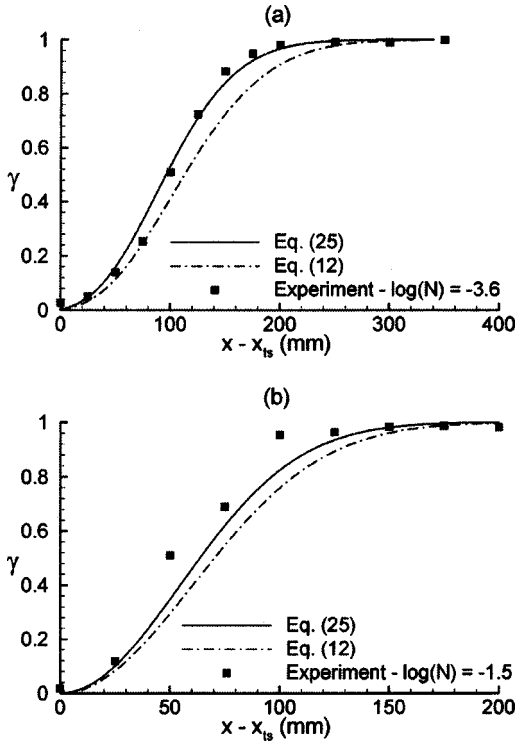

Fig. 9 Intermittency distributions for two attached-flow transition cases (as labeled in Fig. 6)

the cross-stream distribution of velocity as described by the shape factor, surface roughness has a more direct effect. This is an intuitive result, for the sweep and ejection processes leading to generation of turbulent spots take place deep within the boundary layer where they can be readily affected by the local flow perturbations created by the roughness elements. A fairly consistent trend of increasing N with increasing rms roughness height was observed by the authors for the data points displayed in Fig. 6. However, further experiments are desirable before an extension of the proposed correlation for N may be attempted to include rough surface conditions in the attached-flow transition regime.

Finally, as shown in Fig. 6, the spot production rate in instances of separation-bubble transition does not appear to be sensitive to surface roughness, with the exception of two data points. In the majority of the separated-flow transition cases shown in this figure, the separated shear layer was determined to be well above the crests of the roughness elements in the vicinity of the streamwise location of transition inception. Thus, the process leading to the generation of turbulent spots is not expected to be affected by the flow perturbations of the roughness elements to the same extent as in instances of attached-flow transition. This may be the explanation for the lack of sensitivity of the spot production rate to surface roughness in these cases. Consequently, for surface roughness conditions typical of in-service gas turbine blades, the proposed model for predicting the length of the transition zone remains applicable for the separated-flow regime.

Conclusions

Through analysis of an extensive experimental data set, a strong correlation of the turbulent spot production rate with the boundary layer shape factor is identified. Based on this observation, a unified model is proposed for predicting the spot production rate in separated- and attached-flow regimes, for both favorable and adverse streamwise pressure gradients and a range of freestream turbulance levels. The model is shown to maintain the prediction accuracy of an existing model for the attached-flow regime and is the first to allow prediction of the spot production rate in the separated regime. Additionally, in the separated-flow transition regime, the model is shown to remain applicable for rough surface conditions typical of turbomachinery blades.

The model proposed for predicting the length of the transition zone is complemented by a model for locating the streamwise position of transition inception in separation bubbles. The proposed model provides improvements over existing alternatives both in terms of the precision of the predictions, and in its ability of accounting for the effects of freestream turbulence and surface roughness.

Acknowledgments

The authors wish to acknowledge the financial support of Pratt & Whitney Canada in this project. The cooperation of Professor R. J. Volino (U.S. Naval Academy) and Professor J. Dey (Indian Institute of Science) in providing the experimental data for the present comparisons is also greatly appreciated.

Nomenclature

C_p = surface static pressure coefficient
g_x, g_z = functions describing the streamwise and spanwise growth of turbulent spots
H = boundary layer shape factor
H_T = predicted boundary layer shape factor based on the experimental data of Thwaites (Eq. (26))
k_{rms} = rms surface roughness height
L = length of test surface ($L=1.22$ m)
N = spot production parameter (Eq. (10))
n = spot production rate, $(\mathrm{ms})^{-1}$
Re_k = Reynolds number based on rms roughness height
Re_s = Reynolds number based on streamwise distance between the leading edge and the separation location (x_s), and the freestream velocity atx_s (U_{es})
Re_x = Reynolds number based on streamwise distance from the leading edge
Re_L = reference Reynolds number $\mathrm{Re}_L = U_{\mathrm{ref}} L/\nu$
Re_θ = Reynolds number based on momentum thickness
TF = Taylor's turbulence factor $TF = Tu_{\mathrm{ref}}(L/\lambda_s)^{0.2}$
Tu = local freestream turbulence intensity (%)
$\mathrm{Tu}_{\mathrm{ref}}$ = reference turbulence intensity (%) measured 10 mm upstream of the test-surface leading edge
Tu = average Tu (%) from the leading edge to x_{ts}
U_e = local freestream velocity, m/s
U_{LE} = turbulent spot leading-edge convection velocity, m/s
U_{ref} = reference velocity, measured 10 mm upstream of the leading edge of the test surface
U_{TE} = turbulent spot trailing-edge convection velocity, m/s
x, y, z = streamwise, wall-normal, and spanwise coordinates
α = turbulent spot spreading half-angle
γ = intermittency of the boundary layer
θ = momentum thickness
η = acceleration parameter $\eta = (\nu/U_e^2)dU_e/dx$
λ_s = integral length scale of turbulence, measured 10 mm upstream of the test-surface leading edge
λ_θ = Thwaites' pressure gradient parameter $\lambda_\theta = (\theta^2/\nu)dU_e/dx$
ν = kinematic viscosity, m^2/s
σ = spot propagation parameter (Eq. (9))

Subscripts

r = reattachment
s = separation
$s-ts$ = denotes the streamwise distance between the separation and transition inception locations
te = transition completion
ts = transition inception

References

[1] Emmons, H. W., 1951, "The Laminar-Turbulent Transition in a Boundary Layer—Part I," J. Aeronaut. Sci. **18**(7), pp. 490–498.
[2] Schubauer, G. B., and Skramstad, H. K., 1948, "Laminar Boundary-Layer Oscillations and Transition on a Flat Plate," NACA TN 909.
[3] Abu-Ghannam, B. J., and Shaw, R., 1980, "Natural Transition of Boundary Layers: The Effects of Turbulence, Pressure Gradient and Flow History," J. Mech. Eng. Sci. **22**(5), pp. 213–228.
[4] Johnson, M. W., and Dris, A., 2000, "The Origin of Turbulent Spots," ASME J. Turbomach., **122**(1), pp. 88–92.
[5] Kachanov, Y. S., 2000, "Three-dimensional Receptivity of Boundary Layers," Eur. J. Mech. B/Fluids **19**, pp. 723–744.
[6] Klebanoff, P. S., Tidstrom, K. D., and Sargent, L. M., 1961, "The Three-dimensional Nature of Boundary-layer Transition," J. Fluid Mech. **12**, pp. 1–42.
[7] Gostelow, J. P., Melwani, N., and Walker, G. J., 1996, "Effects of Streamwise Pressure Gradient on Turbulent Spot Development," ASME J. Turbomach. **118**, pp. 737–743.
[8] Johnson, M. W., and Fashifar, A., 1994, "Statistical Properties of Turbulent Bursts in Transitional Boundary Layers," Int. J. Heat Fluid Flow **15**(4), pp. 283–290.
[9] Narasimha, R., 1985, "The Laminar-Turbulent Transition Zone in the Boundary Layer," Prog. Aerosp. Sci. **22**, pp. 29–80.
[10] Blair, M. F., 1982, "Influence of Free-Stream Turbulence on Boundary Layer Transition in Favorable Pressure Gradients," ASME J. Eng. Power **104**, pp. 743–750.
[11] Volino, R. J., and Hultgren, L. S., 2000, "Measurements in Separated and Transitional Boundary Layers Under Low-Pressure Turbine Airfoil Conditions," ASME Paper No. 2000-GT-0260.
[12] Johnson, M. W., and Ercan, A. H., 1997, "Predicting Bypass Transition: A Physical Model Versus Empirical Correlations," ASME Paper No. 97-GT-475.
[13] Roberts, S. K., and Yaras, M. I., 2003, "Measurements and Prediction of Free-Stream Turbulence and Pressure-Gradient Effects on Attached-Flow Boundary-Layer Transition," ASME Paper No. GT-2003-38261.
[14] Fraser, C. J., Higazy, M. G., and Milne, J. S., 1994, "End-Stage Boundary Layer Transition Models for Engineering Calculations," Proc. Inst. Mech. Eng., Part C: J. Mech. Eng. Sci. **208**, pp. 47–58
[15] Gostelow, J. P., and Blunden, A. R., 1989, "Investigations of Boundary Layer

Transition in an Adverse Pressure Gradient," ASME J. Turbomach. **111**, pp. 366–375.
[16] Sharma, O. P., and Wells, R. A., Schlinker, R. H., and Bailey, D. A., 1982, "Boundary Layer Development on Turbine Airfoil Suction Surfaces," ASME J. Eng. Power **104**, pp. 698–706.
[17] Kim, J., Simon, T. W., and Russ, S. G., 1992, "Free-Stream Turbulence and Concave Curvature Effects on Heated, Transitional Boundary Layers," ASME J. Heat Transfer **114**, pp. 338–347.
[18] Schultz, M. P., Volino, R. J., 2001, "Effects of Concave Curvature on Boundary Layer Transition Under High Free-Stream Turbulence Conditions," ASME Paper No. 2001-GT-0191.
[19] Stieger, R. D., and Hodson, H. P., 2003, "The Transition Mechanism of Highly-Loaded LP Turbine Blades," ASME Paper No. GT2003-38304.
[20] Dong. Y., and Cumpsty, N. A., 1990, "Compressor Blade Boundary Layers: Part 2—Measurements With Incident Wakes," ASME J. Turbomach. **112**, pp. 231–240.
[21] Schobeiri, M. T., and Rakde, R. E., 1994, "Effects of Periodic Unsteady Wake Flow and Pressure Gradient on Boundary Layer Transition Along the Concave Surface of a Curved Plate," ASME Paper No. 94-GT-327.
[22] Cummings, M. J., and Bragg, M. B., 1996, "Boundary-Layer Transition Due to Isolated Three-Dimensional Roughness on an Airfoil Leading Edge," AIAA J. **34**(9), pp. 1949–1952.
[23] Pinson, M. W., and Wang, T., 1997, "Effects of Leading-edge Roughness on Fluid Flow and Heat Transfer in the Transitional Boundary Layer Over a Flat Plate," Int. J. Heat Mass Transfer **40**(12), pp. 2813–2823.
[24] Lang, M., Rist, U., and Wagner, S., 2004, "Investigations on Controlled Transition Development in a Laminar Separation Bubble by Means of LDA and PIV," Exp. Fluids, **36**, pp. 43-52.
[25] Alam, M., and Sandham, N. D., 2000, "Direct Numerical Simulation of Short Laminar Separation Bubbles With Turbulent Reattachment," J. Fluid Mech. **410**, pp. 1–28.
[26] Rai, M. M., and Moin, P., 1993, "Direct Numerical Simulation of Transition and Turbulence in a Spatially Evolving Boundary Layer," J. Comput. Phys. **109**, pp. 169–192.
[27] Maucher, U., Rist, U., Kloker, M., and Wagner, S., 1999, "DNS of Laminar-Turbulent Transition in Separation bubbles," *High Performance Computing in Science and Engineering '99*, E. Krause, and W. Jäger, eds., Springer-Verlag, New York, pp. 279–294.
[28] Ducros, F., Comte, P., and Lesieur, M., 1996, "Large-Eddy Simulation of Transition to Turbulence in a Boundary Layer Developing Spatially Over a Flat Plate," J. Fluid Mech. **326**, pp. 1–36.
[29] Wilcox, D. C. (1977), "A Model for Transitional Flows," AIAA 77-126.
[30] Rodi, W., and Sheuerer, G., 1985, "Calculation of Laminar-Turbulent Boundary Layer Transition on Turbine Blades," *AGARD Conference Proceedings No.* 390, pp. 18.1–18.13.
[31] Schmidt, R. C., Patankar, S. V., 1991, "Simulating Boundary Layer Transition With Low-Reynolds-Number $k-\varepsilon$ Turbulence Models: Part 1—An Evaluation of Prediction Characteristics," ASME J. Turbomach. **113**, pp. 10–17.
[32] Savill, A. M., 1992, "Evaluating Turbulence Model Predictions of Transition—An ERCOFTAC SIG Project," Appl. Sci. Res. **51**, p. 555.
[33] Savill, A. M., 1993, "Some Recent Progress in the Turbulence Modeling of By-pass Transition" *Near-Wall Turbulent Flows*, R. M. C., So, B. E. Speziale and B. E. Launder (eds.), Elsevier Science, New York, pp. 829–848.
[34] Hobson, G. V., and Weber, S., 2000, "Prediction of a Laminar Separation Bubble Over a Controlled-Diffusion Compressor Blade," ASME Paper No. 2000-GT-277.
[35] Spalart, P. R, and Allmaras, S. R., 1992, "A One-Equation Turbulence Model for Aerodynamic Flows," AIAA 92-0439.
[36] Solomon, W. J., Walker, G. J., and Gostelow, J. P., 1996, "Transition Length Prediction for Flows With Rapidly Changing Pressure Gradients," ASME J. Turbomach. **118**, pp. 744–751.
[37] Steelant, J., and Dick, E., 1996, "Modeling of Bypass Transition With Conditioned Navier-Stokes Equations Coupled to an Intermittency Transport Equation," Int. J. Numer. Methods Eng. **23**, pp. 193–220.
[38] Suzen, Y. B., and Huang, P. G., 2000, "An Intermittency Transport Equation for Modeling Flow Transition," AIAA 2000-0287.
[39] Lesieur, M., and Métais, O., 1996, "New Trends in Large-Eddy Simulations of Turbulence," Annu. Rev. Fluid Mech., pp. 45–82.
[40] Rodi, W., Gerziger, J. H., Breuer, M., and Pourquié, M., 1997, "Status of Large Eddy Simulation: Results of a Workshop," ASME J. Fluids Eng. **119**, pp. 248–262.
[41] Huai, X, Joslin, R. D., and Piomelli, U., 1997, "Large-Eddy Simulation of Transition to Turbulence in Boundary Layers," Theor. Comput. Fluid Dyn. **9**, pp. 149–163.
[42] Chong, T. P., and Zhong, S., 2003, "On the Three-Dimensional Structure of Turbulent Spots," ASME Paper No. GT-2003-38435.
[43] Schubauer, G. B., and Klebanoff, P. S., 1955, "Contributions on the Mechanics of Boundary-Layer Transition," NACA TN 3489.
[44] Hatman, A., and Wang, T., 1999, "A Prediction Model for Separated Flow Transition," ASME J. Turbomach. **121**, pp. 594–602.
[45] Yaras, M. I., 2001, "Measurements of the Effects of Pressure-Gradient History on Separation-Bubble Transition," ASME Paper No. 2001-GT-0192.
[46] Lou, W., and Hourmouziadis, J., 2000, "Separation Bubbles Under Steady and Periodic-Unsteady Main Flow Conditions," ASME Paper No. 2000-GT-0270.
[47] Volino, R. J., and Simon, T. W., 1995, "Bypass Transition in Boundary Layers Including Curvature and Favorable Pressure Gradient Effects," ASME J. Turbomach. **117**, pp. 166–174.
[48] Gostelow, J. P., Blunden, A. R., and Walker, G. J., 1994, "Effects of Free-Stream Turbulence and Adverse Pressure Gradients on Boundary Layer Transition," ASME J. Turbomach. **116**, pp. 392–404.
[49] Zhong, S., Chong, T. P., and Hodson, H. P., 2002, "On the Spreading Angle of Turbulent Spots in Non-Isothermal Boundary Layers With Favourable Pressure Gradients," ASME Paper No. GT-2002-30222.
[50] Mayle, R. E., 1991, "The Role of Laminar-Turbulent Transition in Gas Turbine Engines," ASME J. Turbomach. **113**, p. 509–537.
[51] Roberts, W. B., 1975, "The Effect of Reynolds Number and Laminar Separation on Axial Cascade Performance," ASME J. Eng. Power **97**, pp. 261–274.
[52] Taylor, G. I., 1939, "Some Recent Developments in the Study of Turbulence," *Proc. of 5th Int. Congress Appl. Mech.*, J. P. Den Hartog and H. Peters, eds., Wiley, New York, pp. 294–310.
[53] Yaras, M. I., 2002, "Measurements of the Effects of Freestream Turbulence on Separation-Bubble Transition," ASME GT-2002-30232.
[54] Roberts, S. K., and Yaras, M. I., 2003, "Effects of Periodic-Unsteadiness, Free-Stream Turbulence and Flow Reynolds Number on Separation-Bubble Transition," ASME Paper No. GT-2003-38262.
[55] Gostelow, J. P., and Ramachandran, R. M., 1983, "Some Effects of Free Stream Turbulence on Boundary Layer Transition," *Proc. of 8th Australasian Fluid Mech. Conf.*, Newcastle University, Newcastle, NSW, Australia, pp. 12C.1–12C.4
[56] Devasia, K. J., 1974, "A Study of the Effect of Pressure Gradients on Transition in the Boundary Layer on a Flat Plate," M. Eng. Thesis, Dept. of Aeronautical Eng., Ind. Inst. of Sci., Bangalore, India.
[57] Chen, K. K., and Thyson, N. A., 1971, "Extension of Emmons' Spot Theory to Flows on Blunt Bodies," AIAA J. **5**, pp. 821–825.
[58] Walker, G. J., Subroto, P. H., and Platzer, M. F., 1988, "Inviscid Interaction Analysis of Low Reynolds Number Airfoil Flows Involving Laminar Separation Bubbles," ASME Paper No. 88-GT-32.
[59] D'Ovidio, A., Harkins, J. A., and Gostelow, J. P., 2001, "Turbulent Spots in Strong Adverse Pressure Gradients Part 2—Spot Propagation and Spreading Rates," ASME Paper No. 2001-GT-0406.
[60] Volino, R. J., 2002, "Separated Flow Transition under Simulated Low-Pressure Turbine Airfoil Conditions—Part 1: Mean Flow and Turbulence Statistics," ASME J. Turbomach. **124**, pp. 645–655.
[61] Gostelow, J. P., and Thomas, R. L., 2005, "Response of a Laminar Separation Bubble to an Impinging Wake." ASME J. Turbomach., **127**, pp. 35–42.
[62] Volino, R. J., Shultz, M. P., and Pratt, C. M., 2001, "Conditional Sampling in a Transitional Boundary Layer Under High Free-Stream Turbulence Conditions," ASME Paper No. 2001-GT-0192.
[63] Roberts, S. K., and Yaras, M. I, 2004, "Boundary-Layer Transition Over Rough Surfaces With Elevated Free-Stream Turbulence," ASME Paper No. GT2004-53668.
[64] Roberts, S. K., and Yaras, M. I., 2004, "Effects of Surface Roughness on Boundary-Layer Transition in Separation-Bubbles," ASME Paper No. GT2004-53667.
[65] Dey, J., and Narasimha, R., 1988, "An Integral Method for the Calculation of 2-D Transitional Boundary Layers," Report 88 FM 7, Indian Inst. of Sci., Bangalore, India.
[66] Thwaites, B., 1949, "Approximate Calculation of the Laminar Boundary Layer," Aeronaut. Q. **7**(1), pp. 245–280.
[67] White, F. M., 1991, *Viscous Fluid Flow*, 2nd Ed., McGraw-Hill, New York, p. 614.